INVESTIGATING LARGE-SCALE STRUCTURES IN TURBULENT MIXING LAYERS USING TWO-POINT CORRELATION

Trung Dung Nguyen[1,*], Anh Tuan Nguyen[1], The Hung Tran[1]

[1]*Faculty of Aerospace Engineering, Le Quy Don Technical University*

Abstract

The formation and development of large-scale structures are primary research subjects in the study of turbulent mixing layers. Visualizing these structures based on published experimental data enhances the understanding of complex flow behaviors, which is the main objective of this article. The authors employed a two-point statistical correlation method to evaluate the size of large vortex structures along the interaction region. Additionally, the article provides a guide for analyzing the turbulent energy spectrum at selected fixed points. The calculations were performed using MATLAB software. The results indicate that at the beginning of the mixing layer, the vortices are small and highly anisotropic, with large-scale structures stretching in irregular directions. Further downstream, the vortices increase in size in all directions, and the degree of anisotropy decreases. In the self-similar region, isotropic states are almost achieved. The energy spectrum analysis findings align with Kolmogorov's theory of energy cascade in turbulent flow. The two-point statistical correlation method proves to be highly effective for analyzing structures within turbulent flows.

Keywords: *Two-point correlation; spectrum energy; turbulent length scale; turbulent mixing layer.*

1. Introduction

In recent decades, turbulent mixing layers (TML) have always been an interesting research subject due to their prevalence in nature and engineering [1]. TML are formed when the interaction occurs between two parallel fluid streams moving at different velocities. A key characteristic of TML is that it forms and expands without artificial factors [2]. TML is a core phenomenon in the combustion chambers of scramjet engine [3] and in the exhausted jet behind rocket engines [4], thus research on supersonic vehicles, passenger noise experience [5], and rocket stability motivates efforts to explore the nature of turbulent mixing layers.

TML has been studied through both experimental and numerical methods. In 1974, Brown and Roshko [6] observed large vortex structures in Kelvin-Helmholtz vortices. These vortices formed and moved downstream of the interaction region (Fig. 1a) with the size of the vortices increasing. According to Kolmogorov's Turbulence Theory [7, 8],

[*] Corresponding author, email: dungnt42ncs@lqdtu.edu.vn
DOI: 10.56651/lqdtu.jst.v19.n03.813

turbulent flow consists of a broad range of eddy sizes, where large-scale structures are the main carriers of flow energy. Kinetic energy is transferred from larger eddies to smaller ones and dissipated or converted into heat due to the effect of molecular viscosity. Recognizing that large-scale structures are key to explaining the behaviors of the mixing layers, further studies have focused on describing these large-scale structures. Many studies on large-scale structures using different methods, including experimental (Exp), direct numerical simulation (DNS), and large eddy simulation (LES), are summarized in Table 1. Various types of structures in the mixing layers are shown in Fig. 1b.

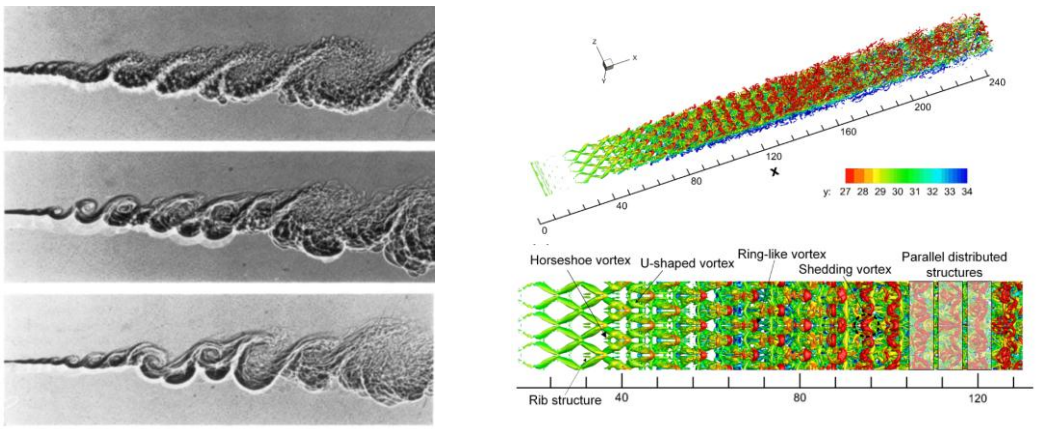

(a) *(b)*

Fig. 1. The large-scale structures in the mixing layers
(a) Shadowgraphs of mixing layer by Brown and Roshko, 1974 [6]*;*
(b) Visualization of eddy structures by Zhang et al., 2019 [9].

Durbin highlighted in his book that the turbulence problem is not a matter of physical law, but rather a problem of description [10]. Analyzing turbulent flow through numerical or experimental methods inevitably leads to a statistical description. Typically, this involves a dataset of velocity fields at discrete points in space and at different times. Due to the statistical and discrete nature of the dataset, methods based on statistical theory and matrix algebra are particularly suitable for studying turbulent flow. Townsend pointed out that a notable characteristic of turbulent motion is that it is less random than chaotic gaseous environments, due to the influence of the pressure field on the motion of fluid particles [11]. Therefore, when analyzing turbulent flow, in addition to accurately describing variables at a single point, it is also necessary to consider the relationship of variables between points in the flow environment.

Table 1. Summary of the large-scale structures in the shear mixing layers

Research, Year	**Method**	**Results**
Brown & Roshko [6], 1974	Exp	- For flow with low Reynolds number the large eddies are two-dimensional. - The spacing between vortex rollers increases with increasing distance downstream.
Sandham & Reynolds [16], 1991	LES	- Identified the inclined Λ-vortex in the temporal simulations at M_C = 0.8.
Clemens & Mungal [17], 1995	Exp	- The mixing layer becomes highly three-dimensional with the increasing convective Mach number M_C.
Fu *et al.* [18], 2000	DNS	- The development of structures in mixing layers goes from the formation of Λ-vortices, through horseshoe vortices and mushroom structures to the smaller vortices of the fully turbulent state.
Qibing Li *et al.* [19], 2003	LES	- Distance for the large-scale vortex development increases with convective Mach number M_C.
Fu & Li [20], 2006	LES	- Oblique structures are more prevalent in the flow with higher M_C.
Liu & Chen [21], 2010	DNS	- The ring-like vortices generation is caused by the interaction between the Λ-shaped vortex tube and streamwise vortices. - The multiple ring-like vortex generation follows the first Helmholtz vortex conservation law.
Zhou *et al.* [22], 2012	DNS	- Λ-vortices, hairpin vortices, and 'flower' structures are populated in the transition process of the flow fields. - Hairpin vortices play an important role in the breakdown of the flow.
Yang *et al.* [23], 2019	DNS	- The large-scale structures in the subsonic-supersonic shear mixing layers formed the small structure earlier. - The Λ eddy and hairpin eddy can be observed, and Λ eddy structure is elongated with the increase of Mc.
Zhang *et al.* [9], 2019	DNS	- The presence of multiple ring-like vortices leads to local strong ejection and sweep regions. - The appearance of multiple ring-like vortices and their evolution can significantly promote mixing in the transition stage.
Chong *et al.* [24], 2021	DNS	- Multiple necklace-like vortices evolve from the Λ-vortices.

Lars Davidson [12], in his lecture notes, defined the term 'correlation' as the tendency of two values or variables to change together, either similarly or oppositely. Additionally, a two-point correlation is analogous to the covariance of two statistical ensembles. In turbulent flow, two-point correlation encompasses various correlation coefficients corresponding to different pairs of variables at two points in the spatial

domain under investigation. Many kinds of two-point correlation coefficients have been studied, such as velocity-velocity correlation, velocity-vorticity correlation, and other correlation conditions used in publications by Sillero and Jimenez [13], Chen *et al.* [14], and Hwang [15]. These analytical techniques are used to highlight the behaviors of large-scale structures in turbulent flow, with characteristics such as shape, size, and position. In turbulent flow research, two-point statistical correlations are used to determine the integral length scales of eddie structures, analyze the energy spectrum, and evaluate the dissipation rate from the perspective of Kolmogorov's Turbulent Theory.

There are two concepts involving two-point statistical correlation: temporal correlation and spatial correlation. Temporal correlation, also known as autocorrelation, essentially considers the correlation of two variables at the same location but at different times. The temporal correlation coefficient is used to determine the integral time scale, while the spatial correlation coefficient is used to determine the integral length scale and energy spectrum.

In this article, the authors focus on using two-point correlation to study large structures in the mixing layers. We specifically employ the spatial correlation coefficients of two variables at distinct locations to determine the length scale, assess changes in the size of vortices, and define the energy spectrum. While Kim *et al.* also used this method to study large vortex structures in 2020 [25], their focus was limited to vortex structures in the self-similar region. In contrast, we chose to investigate both the transition region and the self-similar region, allowing us to evaluate changes in large vortex structures from the initial stage to the point when the flow reaches a fully turbulent state.

The experimental data used for the calculations in this paper were sourced from the publication by Kim *et al.* [26], specifically the SPIV velocity field data, which is accessible online. The calculations in this study were performed using algorithms and MATLAB code developed by the authors themselves. The results provide analyses and evaluations of turbulent organization, enhancing the understanding and knowledge of turbulent mixing layers.

2. Computational method

2.1. Two-point correlation

We use the two-point correlation function presented by Pope [27] in his book as follows:

$$R_{ij}(\overrightarrow{\Delta r},t) \equiv \left\langle u_i\left(\vec{r},t\right)u_j(\vec{r}+\overrightarrow{\Delta r},t)\right\rangle \quad (1)$$

where u_i, u_j (i, j = 1, 2, 3) denote the velocity fluctuations; $\vec{r} = \vec{e_1} \cdot x + \vec{e_2} \cdot y + \vec{e_3} \cdot z$ and $\left(\vec{r} + \overrightarrow{\Delta r}\right)$ are reference location vectors for two distinct points; the numbered indices (i, j = 1, 2, 3) respectively indicate the streamwise (x-direction), transverse (y-direction) and spanwise (z-direction); $\vec{e_i}$ denote the unit vector of the i-direction; $\langle \cdot \rangle$ denote an ensemble average. There are one-dimensional spatial correlation and two-dimensional spatial correlation, with $\overrightarrow{\Delta r} = \vec{e_1} \cdot \Delta x$ or $\overrightarrow{\Delta r} = \vec{e_2} \cdot \Delta y$ for the first, $\overrightarrow{\Delta r} = \vec{e_1} \cdot \Delta x + \vec{e_2} \cdot \Delta y$ and for the other. When using notation without numerical indices, the velocity fluctuation vector can be understood in the form $\vec{u}(u,v,w) \equiv \vec{u}(u_1, u_2, u_3)$. Note that some documents use u', v', and w' to denote velocity fluctuation components.

One-dimensional spatial correlation is used to define the size of the largest eddies in the turbulent field, it is useful to call integral length scale. If two points are located in the x-direction, the correlation is called the longitudinal correlation coefficient

$$C_{uux} = \frac{\langle u(x,y)u(x+\Delta x, y)\rangle}{\sqrt{\langle u^2(x,y)\rangle}\sqrt{\langle u^2(x+\Delta x, y)\rangle}} \tag{2}$$

and the longitudinal integral length scale for components of velocity u-u:

$$L_{uux} = \int_0^\infty C_{uux}(x)dx \tag{3}$$

Similarly, we can define the transverse spatial correlation coefficient and the transverse integral length scale for components of velocity u-u.

$$C_{uuy} = \frac{\langle u(x,y)u(x, y+\Delta y)\rangle}{\sqrt{\langle u^2(x,y)\rangle}\sqrt{\langle u^2(x, y+\Delta y)\rangle}} \tag{4}$$

$$L_{uuy} = \int_0^\infty C_{uuy}(y)dy \tag{5}$$

By substituting the u-u velocity components with v-v velocity components in expressions from (2) to (5), we can define C_{vvx}, C_{vvy}, L_{vvx}, and L_{vvy} for the variable pair of v-v velocity components.

Two-dimensional spatial correlation coefficients for components of velocity *u*-*u* and *v*-*v* follow experssions (6) and (7), respectively.

$$C_{uu} = \frac{\langle u(x,y)u(x+\Delta x, y+\Delta y)\rangle}{\sqrt{\langle u^2(x,y)\rangle}\sqrt{\langle u^2(x+\Delta x, y+\Delta y)\rangle}} \tag{6}$$

$$C_{vv} = \frac{\langle v(x,y)v(x+\Delta x, y+\Delta y)\rangle}{\sqrt{\langle v^2(x,y)\rangle}\sqrt{\langle v^2(x+\Delta x, y+\Delta y)\rangle}} \tag{7}$$

2.2. Energy spectra

Most experimental flow field data is typically obtained in a plane, making the one-dimensional energy spectra the primary focus of analysis. In this article, the authors exclusively analyze the one-dimensional energy spectra. With the magnitude of wavenumber κ, Pope [27] pointed out the relation between turbulent kinetic energy k and energy spectrum function $E(\kappa)$:

$$k = \int_0^\infty E(\kappa)d\kappa \tag{8}$$

The one-dimensional spectra $E_{ij}(\kappa_1)$ are defined to be twice the one-dimensional Fourier transform of the one-dimensional velocity correlation $R_{ij}(e_1 r_1)$. This is the formula (6.206) in the Pope's book [27].

$$E_{ij}(\kappa_1) \equiv \frac{1}{\pi}\int_{-\infty}^{\infty} R_{ij}(e_1 r_1)e^{-i\kappa_1 r_1}dr_1 \tag{9}$$

where number index 1 indicates the streamwise direction (x-direction), and $e_1 r_1 \equiv x$. From (9) rewrite the expansion for longitudinal energy spectra with variable couple *u*-*u* as below:

$$E_{uux}(\kappa_x) \equiv \frac{2}{\pi}\int_0^\infty R_{uux}(x)e^{-i\kappa_x x}dx \tag{10}$$

where $\kappa_x = \kappa_1$ is the wave number versus the x-direction.

The experimental data obtained is discrete, we can perform a Fast Fourier Transform (*FFT command*) in MATLAB, from which it is easy to obtain one-dimensional energy spectra.

2.3. Experimental data

In 2019, Kim and colleagues investigated the compressibility effects on turbulent free shear layers [26]. The experimental data were published for five cases with convective Mach number ranging from M_C = 0.185 to 0.883, and now available online. In these experiments, Kim used stereoscopic particle image velocimetry (SPIV) to obtain three velocity component measurements on the two-dimensional vertical symmetry plane. In this paper, the authors have chosen experiment data from the first case of Kim with M_C = 0.185. The dataset is divided into 4 field-of-views (FOV). Each FOV has about 3000+ sample statistical velocity components at fixed points.

To facilitate the calculation steps in MATLAB, we create a uniform grid to standardize the experimental data with spacing $\Delta x = \Delta y = 0.25$ mm. Use the command *griddata* in MATLAB to interpolate the experimental statistical data into numerical data on the new grid. After this step, the velocity component matrices are obtained. Note that velocity component matrices are three-dimensional, the third dimensional of these matrices indicates the velocity value as time series. With the *mean* command in MATLAB, the average flow is easily calculated. Figure 2 shows the color contour of the streamwise average velocity, highlighting the interaction area between the two black lines. The determination of the centerline and the shear thickness of the mixing layer follows the methodology presented by Kim [26]. The centerline of the interaction area y_0, and the width of the interaction area b, vary in the x-direction. Four positions along the centerline of the mixing layer along the streams are selected for the study, and these selected points are also shown in Fig. 2.

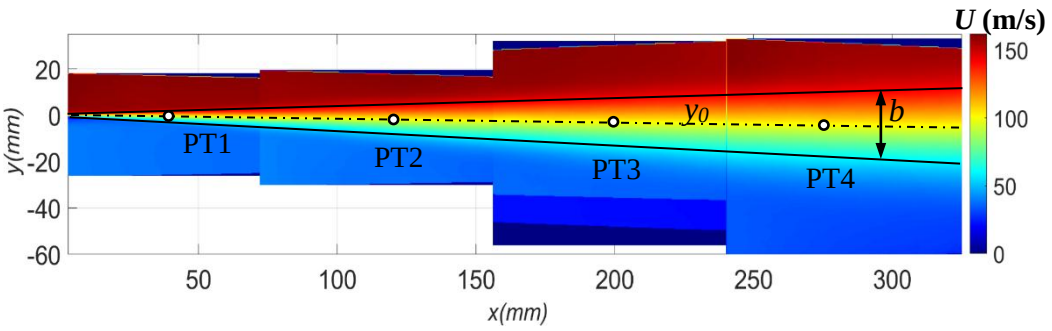

Fig. 2. Average streamwise velocity distribution with selection points.

Here, the authors have identified the centerline y_0, and the shear thickness b, selected the appropriate points for further calculations, and summarized them in Table 2.

Table 2. Chosen local positions for investing

Local points	**PT1**	**PT2**	**PT3**	**PT4**
x, mm	40	120	200	290
y_0, mm	-0.08	-3.50	-5.88	-8.25
b, mm	5.50	16.00	27.50	39.50

3. Results and discussions

3.1. Instantaneous vortical analysis

According to Brown and Roshko [6], with incident lines with low Reynolds numbers, eddy structures take the form of Kelvin-Helmholtz in a spanwise direction. Therefore considering spanwise vorticity is a suggestion to make first. The spanwise vorticity can be determined as

$$\omega_z = \frac{1}{2}\left(\frac{\partial U}{\partial y} - \frac{\partial V}{\partial x}\right) \tag{11}$$

where U and V denote the instantaneous velocity components in the x-direction and y-direction, respectively. With the *curl* command in MATLAB, it is quick to determine the spanwise vorticity magnitude $|\omega_z|$ with the data under consideration. Figure 3 shows the instantaneous spanwise vorticity magnitude distribution at times $t = 2.0\cdot10^{-3}$ s, $2.4\cdot10^{-3}$ s, and $2.8\cdot10^{-3}$ s.

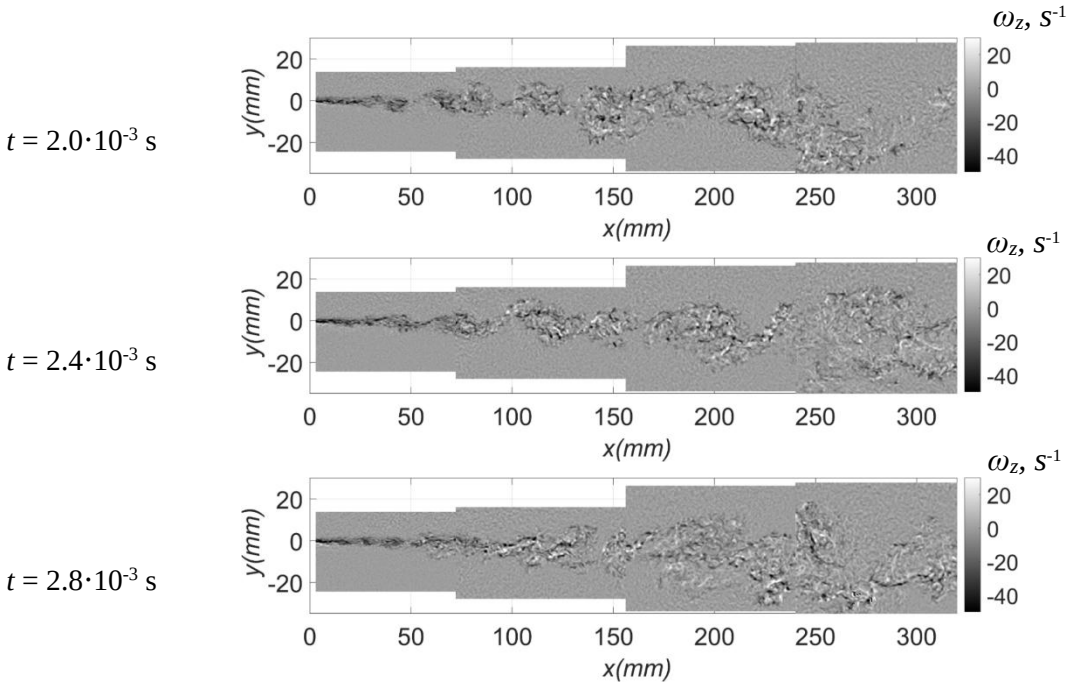

Fig. 3. Instantaneous vorticity in the mixing layer with M_C = 0.185.

These images in Fig. 3 indicate the existence of large structures in the mixing layer. The vortex rollers form and grow downstream. Towards the downstream region, the contrast by the vortex decreases, indicating that the anisotropy level decreases downstream.

3.2. One-dimensional spatial velocity correlation

To calculate the longitudinal and transverse correlation for the variable pairs *u*-*u* and *v*-*v*, select the same distances $Lx = Ly = 20$ mm along the *x*-direction and *y*-direction from selected points PT1-PT4. By applying formulas (2) and (4), we determine the longitudinal and transverse correlation coefficients at each selected point, resulting in the graphs shown in Fig. 4.

We already know that vortex size can be estimated through the integral length scale defined by formulas (3) and (5). However, performing a defined integral with supremum at infinity is challenging. Various methods exist for determining the integral length, one of which is the zero-crossing method employed in this case. Consequently, the integral length value is defined as the area below the graph of correlation coefficients, bounded by a zero-degree maturity line.

All graphs in Fig. 4 demonstrate an increasing vortex size along the flow from the PT1-PT4 point. For the *u*-*u* variable pair, both longitudinal and transverse correlations increase simultaneously with the flow direction from PT1-PT4, indicating that the streamwise velocity component affects the surrounding area in both streamwise and transverse directions. On the other hand, the *v*-*v* variable pair exhibits increased longitudinal correlation (Fig. 4c), while the transverse correlation (Fig. 4d) from the PT2-PT4 point remains nearly constant, suggesting that structures do not tend to develop in the transverse (*y*-direction).

To determine the integral length, the authors use the numerical integral calculation method to calculate the lower area of the graphs to the zero-crossing with the *trapz* command in MATLAB. The integral length *L* approximates the largest vortex size at the chosen points. We investigate the *L/b* ratio between integral length scale and shear layer thickness to evaluate vortex size relative to shear layer thickness. Figure 5 shows the *L/b* ratios at different locations according to the flow direction. The results show that the integral length scale at the beginning of the interaction region is highly different. This difference decreases along the flow, at the PT4 position corresponding to the homomorphic region with the slightest difference. This shows that the anisotropy is evident at the beginning of the mixing layer, but with the flow, the inevitability decreases and almost reaches an isotropic state in the self-similar region of the mixing layer.

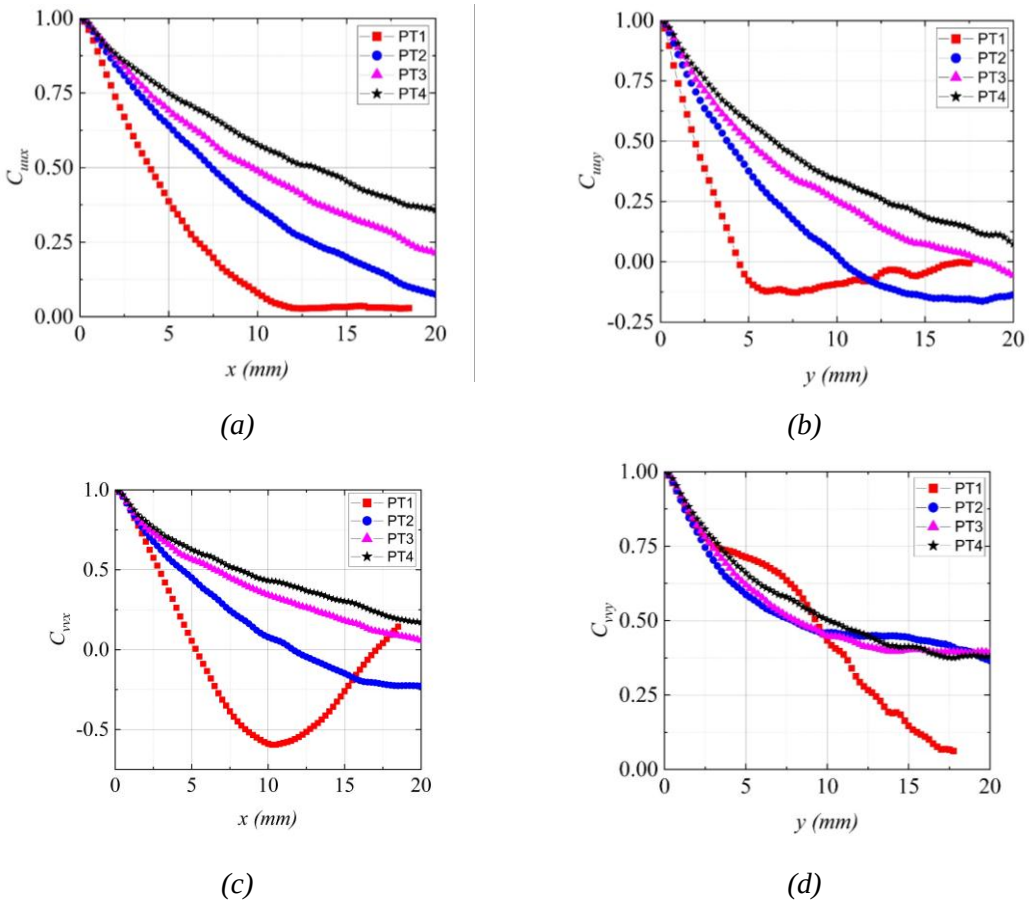

Fig. 4. One-dimensional spatial velocity correlation coefficients
(a) Longitudinal correlation coefficient for u-u; (b) Transverse correlation coefficient for u-u;
(c) Longitudinal correlation coefficient for v-v; (d) Transverse correlation coefficient for v-v.

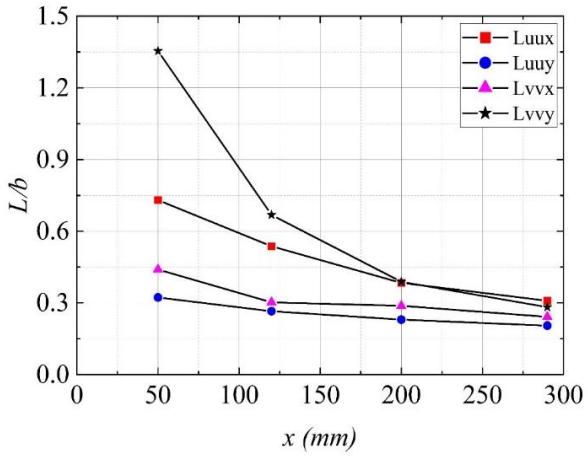

Fig. 5. Ratios of integral length scale and shear layer thickness along streams.

3.3. Two-dimensional spatial velocity correlation

A square box survey area measuring 30 mm × 30 mm and taking the survey point as the center of the square is selected. With the survey area size and experimental data characteristics divided into 4 partitions, the reason for the authors to choose the survey sites is as mentioned. Figure 6 shows the two-dimensional correlation coefficient value distribution of the *u-u* variable pair at the survey sites. An isovalent line equal to 0.3 black is added to figures for easily observing the trends of shapes. Figure 6 shows that the area of correlation regions with selected points has increased downstream but still maintains their shape.

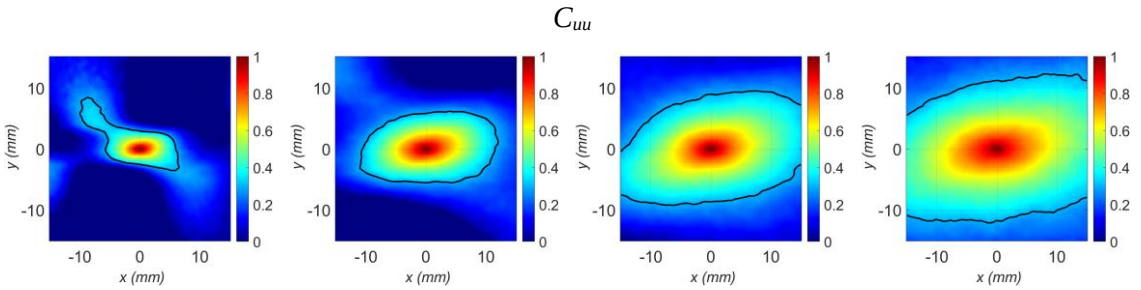

(a) PT1 *(b) PT2* *(c) PT3* *(d) PT4*

Fig. 6. Distribution of two-dimensional velocity correlation coefficients for u-u at positions with a black 0.3 isovalent line

Figure 7 shows the two-dimensional correlation coefficient value distribution of variable pairs *v-v* at the selected points. A black 0.3 isovalent line is also added to the figures. Excluding the PT1 case when the correlation region (Fig. 6a) is overstretched methodically, the PT2-PT4 points have a fairly similar core. The trend of deviation of the distribution of C_{uu} and C_{vv} according to Kim is the mechanism of creating vortex structures on the interaction zone.

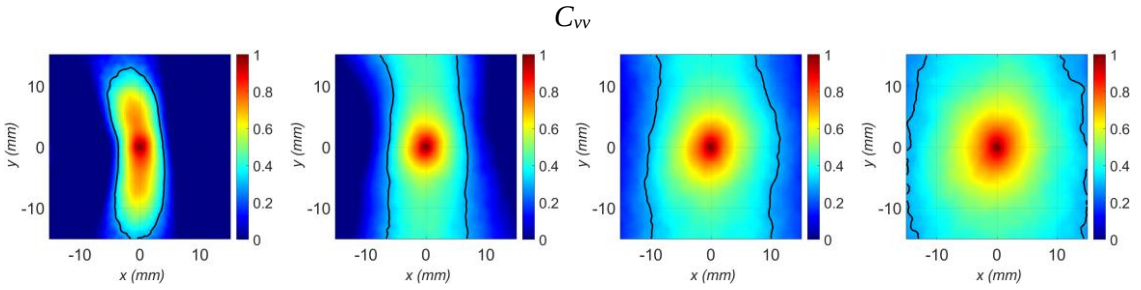

(a) PT1 *(b) PT2* *(c) PT3* *(d) PT4*

Fig. 7. Distribution of two-dimensional velocity correlation coefficients for v-v at positions with a black 0.3 isovalent line.

3.4. Energy spectra

In this section, the longitudinal energy spectra (x-direction) are determined by the formula (6) - (8). With discrete data grids, the smallest vortex size can be determined by the grid distance. That is, the smallest wavelength $\lambda_{min} = 2\Delta x$, and the maximum wavenumber is $\kappa_{max} = 2\pi/\lambda_{min} = \pi/\Delta x$, while the smallest number of waves corresponds to the integral length scale.

Note that, following equation (8) longitudinal energy spectra E_{uux} are obtained by performing the Fast Fourie Transform of correlation function $R_{uux}(x)$. Therefore, it is first necessary to determine the discrete values of the correlation function $R_{uux}(x)$. The steps for calculating discrete $R_{uux}(x)$ are similar to calculating C_{uux} and C_{vvx} in Section 3.3. After that, use the *FFT* tool on MATLAB to obtain the longitudinal energy spectra E_{uux}.

Figure 8 shows the results of the energy spectrum $E_{uux}(\kappa)$ at selected points. The dashed orange line shows the (-5/3) slope. Notice that the graphs show the existence of an inertial region consistent with Kolmogorov's entanglement energy propagation theory.

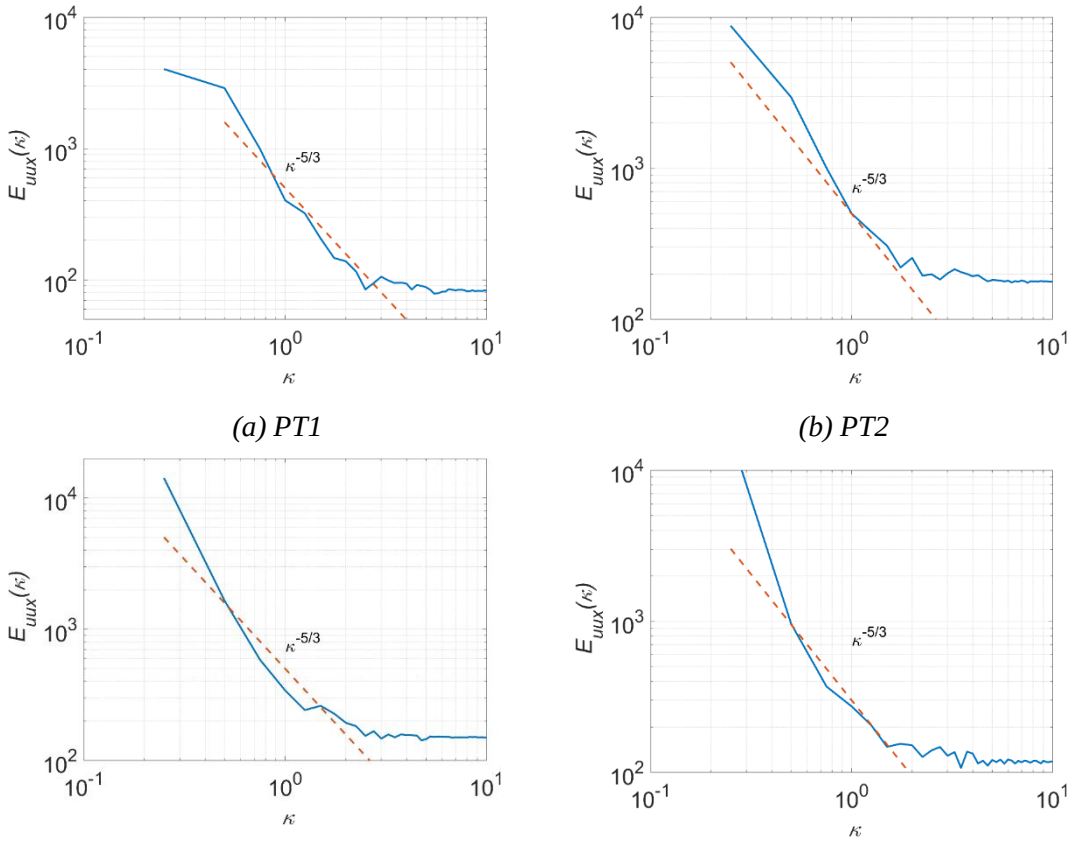

(a) PT1 *(b) PT2*

(c) PT3 *(d) PT4*

Fig. 8. One-dimensional energy spectra at selected positions.

4. Conclusions

For turbulent mixing layers with M_C = 0.185, the results of the article show that the statistical theory of two-point spatial correlation is effective in analyzing the relationship between two components of velocity fluctuation over the turbulent interaction zone. At the beginning of the mixing layer, the vortices are small in size with high anisotropy, showing large structures stretched in irregular directions. Downstream, the vortex size tends to increase in directions accompanied by a decrease in the anisotropy level. In the self-similar region, the interaction zone almost reaches an isotropic state. The displacement trend of C_{uu} and C_{vv} ensures the mechanism of creating vortex structures on the interaction zone. The one-dimensional energy spectrum based on the two-point correlation function is analyzed. The according of energy spectrum with the (-5/3) law is supported by Kolmogorov's Turbulent Theory. This computational procedure is useful for further investigation of turbulent interaction flows with different M_C values. The MATLAB program developed by the authors provides strong support for this research and future studies.

References

[1] D. A. Yoder and N. J. Georgiadis, "Fundamentals of Compressible Turbulent Mixing", in *Encyclopedia of Aerospace Engineering*, John Wiley & Sons, Ltd., 2010, pp. 1-8. DOI: 10.1002/9780470686652.eae031

[2] S. G. Goebel and J. C. Dutton, "Experimental study of compressible turbulent mixing layers", *AIAA Journal*, Vol. 29, No. 4, pp. 538-546, Apr. 1991. DOI: 10.2514/3.10617

[3] J. M. Seiner, S. M. Dash, and D. C. Kenzakowski, "Historical Survey on Enhanced Mixing in Scramjet Engines", *Journal of Propuls Power*, Vol. 17, No. 6, pp. 1273-1286, Nov. 2001. DOI: 10.2514/2.5876

[4] E. Murakami and D. Papamoschou, *Mixing layer characteristics of coaxial supersonic jets*, Jun. 2000, pp. 1-16. DOI: 10.2514/6.2000-2060

[5] L. Zhou, Z. Wan, D. Sun, and M. Wei, "The effects of initial perturbation to mixing-layer noise", *Theoretical and Applied Mechanics Letters*, Vol. 2, No. 3, 2012, 03203. DOI: 10.1063/2.1203203

[6] G. L. Brown and A. Roshko, "On density effects and large structure in turbulent mixing layers", *Journal of Fluid Mechanics*, Vol. 64, No. 4, pp. 775-816, 1974. DOI: 10.1017/S002211207400190X.

[7] A. N. Kolmogorov, "Dissipation of energy under locally isotropic turbulence", *Dokl Akad Nauk SSSR*, Vol. 32, pp. 16-18, 1941.

[8] A. N. Kolmogorov, "The local structure of turbulence in incompressible viscous fluid for very large Reynolds number", *Dokl Akad Nauk SSSR*, Vol. 30, pp. 9-13, 1941.

[9] D. Zhang, J. Tan, and X. Yao, "Direct numerical simulation of spatially developing highly compressible mixing layer: Structural evolution and turbulent statistics", *Physics of Fluids*, Vol. 31, No. 3, Mar. 2019, 036102. DOI: 10.1063/1.5087540

[10] P. A. Durbin and B. Pettersson-Reif, "Chapter 2 - Mathematical and statistical background", in *Statistical Theory and Modeling for Turbulent Flow*, 2nd ed. West Sussex, United Kingdom: Wiley, 2011, pp. 15-44.

[11] A. Townsend, "Chapter 6 - Free turbulent shear flows", in *The Structure of Turbulent Shear Flow*, 2nd ed. Cambridge: Cambridge University Press, 1980, pp, 186-258.

[12] L. Davidson, "Fluid mechanics, turbulent flow and turbulence modeling", Sweden: Chalmers University of Technology, 2020. [Online]. Available: https://api.semanticscholar.org/CorpusID:219810565

[13] J. A. Sillero, J. Jiménez, and R. D. Moser, "Two-point statistics for turbulent boundary layers and channels at Reynolds numbers up to $\delta+ \approx 2000$", *Physics of Fluids*, Vol. 26, No. 10, Oct. 2014, 105109. DOI: 10.1063/1.4899259

[14] Jun Chen, "Two-Point Statistics of Coherent Structure in Turbulent Flow", *Journal of Flow Control, Measurement & Visualization*, Vol. 7, pp. 153-173, 2019.

[15] J. Hwang, J. Lee, H. J. Sung, and T. A. Zaki, "Inner-outer interactions of large-scale structures in turbulent channel flow", *Journal of Fluid Mechanics*, Vol. 790, pp. 128-157, 2016. DOI: 10.1017/jfm.2016.3

[16] N. D. Sandham and W. C. Reynolds, "Three-dimensional simulations of large eddies in the compressible mixing layer", *Journal of Fluid Mechanics*, Vol. 224, pp. 133-158, 1991. DOI: 10.1017/S0022112091001684

[17] N. T. Clemens and M. G. Mungal, "Large-scale structure and entrainment in the supersonic mixing layer", *Journal of Fluid Mechanics*, Vol. 284, pp. 171-216, 1995. DOI: 10.1017/S0022112095000310

[18] D. Fu, Y. Ma, and L. Zhang, "Direct numerical simulation of transition and turbulence in compressible mixing layer", *Science in China Series A: Mathematics*, Vol. 43, No. 4, pp. 421-429, 2000. DOI: 10.1007/BF02897166

[19] Q. Li, H. Chen, and S. Fu, "Large-scale vortices in high-speed mixing layers", *Physics of Fluids*, Vol. 15, No. 10, pp. 3240-3243, Oct. 2003. DOI: 10.1063/1.1602075

[20] S. Fu and Q. Li, "Numerical simulation of compressible mixing layers", *International Journal of Heat and Fluid Flow*, Vol. 27, No. 5, pp. 895-901, Oct. 2006. DOI: 10.1016/j.ijheatfluidflow.2006.03.028

[21] C. Liu and L. Chen, *Study of Mechanism of Ring-Like Vortex Formation in Late Flow Transition*, 2010, pp. 1-21. DOI: 10.2514/6.2010-1456

[22] Q. Zhou, F. He, and M. Y. Shen, "Direct numerical simulation of a spatially developing compressible plane mixing layer: Flow structures and mean flow properties", *Journal of Fluid Mechanics*, Vol. 711, pp. 437-468, 2012. DOI: 10.1017/jfm.2012.400

[23] L. Yang, M. Dong, F. Benshuai, L. Qiang, and Z. Chenxi, "Direct numerical simulation of fine flow structures of subsonic-supersonic mixing layer", *Aerospace Science and Technology*, Vol. 95, 2019, 105431. DOI: 10.1016/j.ast.2019.105431

[24] D. Chong, Y. Bai, Q. Zhao *et al.*, "Direct numerical simulation of vortex structures during the late stage of the transition process in a compressible mixing layer", *Physics of Fluids*, Vol. 33, Iss. 5, May 2021, 054108. DOI: 10.1063/5.0048584

[25] K. U. Kim, G. S. Elliott, and J. C. Dutton, "Compressibility effects on large structures and entrainment length scales in mixing layers", *AIAA Journal*, Vol. 58, No. 12, pp. 5168-5182, 2020. DOI: 10.2514/1.J059433

[26] K. U. Kim, G. S. Elliott, and J. C. Dutton, "Three-dimensional experimental study of compressibility effects on turbulent free shear layers", *AIAA Journal*, Vol. 58, No. 1, pp. 133-147, 2019. DOI: 10.2514/1.J058556

[27] S. B. Pope, "Chapter 6 - The scales of turbulent motion" in *Turbulent Flows*. Cambridge: Cambridge University Press, 2000, pp. 182-263. DOI: 10.1017/CBO9780511840531

NGHIÊN CỨU CÁC CẤU TRÚC LỚN TRONG VÙNG TƯƠNG TÁC CHẢY RỐI BẰNG PHƯƠNG PHÁP TƯƠNG QUAN HAI ĐIỂM

Nguyễn Trung Dũng[1], Nguyễn Anh Tuấn[1], Trần Thế Hùng[1]

[1]*Khoa Hàng không vũ trụ, Trường Đại học Kỹ thuật Lê Quý Đôn*

Tóm tắt: Sự hình thành và phát triển của các cấu trúc xoáy kích thước lớn là một trong các đối tượng nghiên cứu chính về dòng chảy rối trên vùng tương tác. Mục tiêu chính của bài báo này là trực quan hóa các cấu trúc này từ dữ liệu thực nghiệm đã được công bố giúp nâng cao hiểu biết về các hành vi dòng chảy phức tạp. Trong bài báo này, nhóm tác giả sử dụng phương pháp tương quan thống kê hai điểm để đánh giá kích thước các cấu trúc xoáy lớn dọc theo dòng chảy. Bài báo cũng trình bày hướng dẫn phân tích phổ năng lượng rối tại các điểm cố định đã chọn. Các tính toán được thực hiện trên phần mềm MATLAB. Kết quả thu được cho thấy tại khu vực bắt đầu vùng tương tác, các xoáy có kích thước nhỏ với độ bất đẳng hướng cao, các cấu trúc lớn có xu hướng bị kéo căng theo các hướng không đều. Xuôi theo dòng chảy, kích thước các xoáy có xu hướng tăng lên theo các hướng, đồng thời mức độ bất đẳng hướng có xu hướng giảm. Trong vùng đồng dạng, trạng thái đẳng hướng gần như đạt được. Các phát hiện về phân tích phổ năng lượng cho thấy bằng chứng phù hợp với thuyết truyền năng lượng trong dòng chảy rối của Kolmogorov. Phương pháp tương quan thống kê hai điểm thực sự hiệu quả để phân tích về các cấu trúc trong dòng chảy rối.

Từ khóa: *Tương quan hai điểm; phổ năng lượng rối; cấu trúc xoáy lớn; vùng tương tác chảy rối.*

Received: 19/06/2024; Revised: 15/10/2024; Accepted for publicaton: 21/11/2024

❑